

Hadronization geometry and charge-dependent number autocorrelations on axial momentum space in Au-Au collisions at $\sqrt{s_{NN}} = 130$ GeV

J. Adams,³ M.M. Aggarwal,²⁹ Z. Ahammed,⁴³ J. Amonett,²⁰ B.D. Anderson,²⁰ D. Arkhipkin,¹³ G.S. Averichev,¹² Y. Bai,²⁷ J. Balewski,¹⁷ O. Barannikova,³² L.S. Barnby,³ J. Baudot,¹⁸ S. Bekele,²⁸ V.V. Belaga,¹² R. Bellwied,⁴⁶ J. Berger,¹⁴ B.I. Bezverkhny,⁴⁸ S. Bharadwaj,³³ V.S. Bhatia,²⁹ H. Bichsel,⁴⁵ A. Billmeier,⁴⁶ L.C. Bland,⁴ C.O. Blyth,³ B.E. Bonner,³⁴ M. Botje,²⁷ A. Boucham,³⁸ A. Brandin,²⁵ A. Bravar,⁴ M. Bystersky,¹¹ R.V. Cadman,¹ X.Z. Cai,³⁷ H. Caines,⁴⁸ M. Calderón de la Barca Sánchez,⁴ J. Carroll,²¹ J. Castillo,²¹ D. Cebra,⁷ Z. Chajecski,⁴⁴ P. Chaloupka,¹¹ S. Chattopdhyay,⁴³ H.F. Chen,³⁶ Y. Chen,⁸ J. Cheng,⁴¹ M. Cherney,¹⁰ A. Chikhanian,⁴⁸ W. Christie,⁴ J.P. Coffin,¹⁸ T.M. Cormier,⁴⁶ J.G. Cramer,⁴⁵ H.J. Crawford,⁶ D. Das,⁴³ S. Das,⁴³ M.M. de Moura,³⁵ A.A. Derevschikov,³¹ L. Didenko,⁴ T. Dietel,¹⁴ W.J. Dong,⁸ X. Dong,³⁶ J.E. Draper,⁷ F. Du,⁴⁸ A.K. Dubey,¹⁵ V.B. Dunin,¹² J.C. Dunlop,⁴ M.R. Dutta Mazumdar,⁴³ V. Eckardt,²³ W.R. Edwards,²¹ L.G. Efimov,¹² V. Emelianov,²⁵ J. Engelage,⁶ G. Eppley,³⁴ B. Erasmus,³⁸ M. Estienne,³⁸ P. Fachini,⁴ J. Faivre,¹⁸ R. Fatemi,¹⁷ J. Fedorisin,¹² K. Filimonov,²¹ P. Filip,¹¹ E. Finch,⁴⁸ V. Fine,⁴ Y. Fisyak,⁴ K.J. Foley,⁴ K. Fomenko,¹² J. Fu,⁴¹ C.A. Gagliardi,³⁹ J. Gans,⁴⁸ M.S. Ganti,⁴³ L. Gaudichet,³⁸ F. Geurts,³⁴ V. Ghazikhanian,⁸ P. Ghosh,⁴³ J.E. Gonzalez,⁸ O. Grachov,⁴⁶ O. Grebenyuk,²⁷ D. Grosnick,⁴² S.M. Guertin,⁸ Y. Guo,⁴⁶ A. Gupta,¹⁹ T.D. Gutierrez,⁷ T.J. Hallman,⁴ A. Hamed,⁴⁶ D. Hardtke,²¹ J.W. Harris,⁴⁸ M. Heinz,² T.W. Henry,³⁹ S. Hepplemann,³⁰ B. Hippolyte,⁴⁸ A. Hirsch,³² E. Hjort,²¹ G.W. Hoffmann,⁴⁰ H.Z. Huang,⁸ S.L. Huang,³⁶ E.W. Hughes,⁵ T.J. Humanic,²⁸ G. Igo,⁸ A. Ishihara,⁴⁰ P. Jacobs,²¹ W.W. Jacobs,¹⁷ M. Janik,⁴⁴ H. Jiang,⁸ P.G. Jones,³ E.G. Judd,⁶ S. Kabana,² K. Kang,⁴¹ M. Kaplan,⁹ D. Keane,²⁰ V.Yu. Khodyrev,³¹ J. Kiryluk,²² A. Kisiel,⁴⁴ E.M. Kislov,¹² J. Klay,²¹ S.R. Klein,²¹ A. Klyachko,¹⁷ D.D. Koetke,⁴² T. Kollegger,¹⁴ M. Kopytine,²⁰ L. Kotchenda,²⁵ M. Kramer,²⁶ P. Kravtsov,²⁵ V.I. Kravtsov,³¹ K. Krueger,¹ C. Kuhn,¹⁸ A.I. Kulikov,¹² A. Kumar,²⁹ C.L. Kunz,⁹ R.Kh. Kutuev,¹³ A.A. Kuznetsov,¹² M.A.C. Lamont,³ J.M. Landgraf,⁴ S. Lange,¹⁴ F. Laue,⁴ J. Lauret,⁴ A. Lebedev,⁴ R. Lednicky,¹² S. Lehocka,¹² M.J. LeVine,⁴ C. Li,³⁶ Q. Li,⁴⁶ Y. Li,⁴¹ S.J. Lindenbaum,²⁶ M.A. Lisa,²⁸ F. Liu,⁴⁷ L. Liu,⁴⁷ Q.J. Liu,⁴⁵ Z. Liu,⁴⁷ T. Ljubicic,⁴ W.J. Llope,³⁴ H. Long,⁸ R.S. Longacre,⁴ M. Lopez-Noriega,²⁸ W.A. Love,⁴ Y. Lu,⁴⁷ T. Ludlam,⁴ D. Lynn,⁴ G.L. Ma,³⁷ J.G. Ma,⁸ Y.G. Ma,³⁷ D. Magestro,²⁸ S. Mahajan,¹⁹ D.P. Mahapatra,¹⁵ R. Majka,⁴⁸ L.K. Mangotra,¹⁹ R. Manweiler,⁴² S. Margetis,²⁰ C. Markert,⁴⁸ L. Martin,³⁸ J.N. Marx,²¹ H.S. Matis,²¹ Yu.A. Matulenko,³¹ C.J. McClain,¹ T.S. McShane,¹⁰ F. Meissner,²¹ Yu. Melnick,³¹ A. Meschanin,³¹ M.L. Miller,²² Z. Milosevich,⁹ N.G. Minaev,³¹ C. Mironov,²⁰ A. Mischke,²⁷ D. Mishra,¹⁵ J. Mitchell,³⁴ B. Mohanty,⁴³ L. Molnar,³² C.F. Moore,⁴⁰ M.J. Mora-Corral,²³ D.A. Morozov,³¹ V. Morozov,²¹ M.G. Munhoz,³⁵ B.K. Nandi,⁴³ T.K. Nayak,⁴³ J.M. Nelson,³ P.K. Netrakanti,⁴³ V.A. Nikitin,¹³ L.V. Nogach,³¹ B. Norman,²⁰ S.B. Nurushev,³¹ G. Odyniec,²¹ A. Ogawa,⁴ V. Okorokov,²⁵ M. Oldenburg,²¹ D. Olson,²¹ S.K. Pal,⁴³ Y. Panebratsev,¹² S.Y. Panitkin,⁴ A.I. Pavlinov,⁴⁶ T. Pawlak,⁴⁴ T. Peitzmann,²⁷ V. Perevoztchikov,⁴ C. Perkins,⁶ W. Peryt,⁴⁴ V.A. Petrov,¹³ S.C. Phatak,¹⁵ R. Picha,⁷ M. Planinic,⁴⁹ J. Pluta,⁴⁴ N. Porile,³² J. Porter,⁴ A.M. Poskanzer,²¹ M. Potekhin,⁴ E. Potrebenikova,¹² B.V.K.S. Potukuchi,¹⁹ D. Prindle,⁴⁵ C. Pruneau,⁴⁶ J. Putschke,²³ G. Rai,²¹ G. Rakness,³⁰ R. Raniwala,³³ S. Raniwala,³³ O. Ravel,³⁸ R.L. Ray,⁴⁰ S.V. Razin,¹² D. Reichhold,³² J.G. Reid,⁴⁵ G. Renault,³⁸ F. Retiere,²¹ A. Ridiger,²⁵ H.G. Ritter,²¹ J.B. Roberts,³⁴ O.V. Rogachevskiy,¹² J.L. Romero,⁷ A. Rose,⁴⁶ C. Roy,³⁸ L. Ruan,³⁶ I. Sakrejda,²¹ S. Salur,⁴⁸ J. Sandweiss,⁴⁸ I. Savin,¹³ P.S. Sazhin,¹² J. Schambach,⁴⁰ R.P. Scharenberg,³² N. Schmitz,²³ L.S. Schroeder,²¹ K. Schweda,²¹ J. Seger,¹⁰ P. Seyboth,²³ E. Shahaliev,¹² M. Shao,³⁶ W. Shao,⁵ M. Sharma,²⁹ W.Q. Shen,³⁷ K.E. Shestermanov,³¹ S.S. Shimanskiy,¹² F. Simon,²³ R.N. Singaraju,⁴³ G. Skoro,¹² N. Smirnov,⁴⁸ R. Snellings,²⁷ G. Sood,⁴² P. Sorensen,²¹ J. Sowinski,¹⁷ J. Speltz,¹⁸ H.M. Spinka,¹ B. Srivastava,³² A. Stadnik,¹² T.D.S. Stanislaus,⁴² R. Stock,¹⁴ A. Stolpovsky,⁴⁶ M. Strikhanov,²⁵ B. Stringfellow,³² A.A.P. Suaide,³⁵ E. Sugarbaker,²⁸ C. Suire,⁴ M. Sumbera,¹¹ B. Surrow,²² T.J.M. Symons,²¹ A. Szanto de Toledo,³⁵ P. Szarwas,⁴⁴ A. Tai,⁸ J. Takahashi,³⁵ A.H. Tang,²⁷ T. Tarnowsky,³² D. Thein,⁸ J.H. Thomas,²¹ S. Timoshenko,²⁵ M. Tokarev,¹² T.A. Trainor,⁴⁵ S. Trentalange,⁸ R.E. Tribble,³⁹ O. Tsai,⁸ J. Ulery,³² T. Ullrich,⁴ D.G. Underwood,¹ A. Urkinbaev,¹² G. Van Buren,⁴ M. van Leeuwen,²¹ A.M. Vander Molen,²⁴ R. Varma,¹⁶ I.M. Vasilevski,¹³ A.N. Vasiliev,³¹ R. Vernet,¹⁸ S.E. Vigdor,¹⁷ V.P. Viyogi,⁴³ S. Vokal,¹² S.A. Voloshin,⁴⁶ M. Vznuzdaev,²⁵ B. Waggoner,¹⁰ F. Wang,³² G. Wang,²⁰ G. Wang,⁵ X.L. Wang,³⁶ Y. Wang,⁴⁰ Y. Wang,⁴¹ Z.M. Wang,³⁶ H. Ward,⁴⁰ J.W. Watson,²⁰ J.C. Webb,¹⁷ R. Wells,²⁸ G.D. Westfall,²⁴ A. Wetzler,²¹ C. Whitten Jr.,⁸ H. Wieman,²¹ S.W. Wissink,¹⁷ R. Witt,² J. Wood,⁸ J. Wu,³⁶ N. Xu,²¹ Z. Xu,⁴ Z.Z. Xu,³⁶ E. Yamamoto,²¹ P. Yepes,³⁴ V.I. Yurevich,¹² Y.V. Zanevsky,¹² H. Zhang,⁴ W.M. Zhang,²⁰ Z.P. Zhang,³⁶ P.A. Zolnierczuk,¹⁷ R. Zoulkarneev,¹³ Y. Zoulkarneeva,¹³ and A.N. Zubarev¹²

(STAR Collaboration)

- ¹Argonne National Laboratory, Argonne, Illinois 60439
²University of Bern, Bern, Switzerland CH-3012
³University of Birmingham, Birmingham, United Kingdom
⁴Brookhaven National Laboratory, Upton, New York 11973
⁵California Institute of Technology, Pasadena, California 91125
⁶University of California, Berkeley, California 94720
⁷University of California, Davis, California 95616
⁸University of California, Los Angeles, California 90095
⁹Carnegie Mellon University, Pittsburgh, Pennsylvania 15213
¹⁰Creighton University, Omaha, Nebraska 68178
¹¹Nuclear Physics Institute AS CR, 250 68 Řež/Prague, Czech Republic
¹²Laboratory for High Energy (JINR), Dubna, Russia
¹³Particle Physics Laboratory (JINR), Dubna, Russia
¹⁴University of Frankfurt, Frankfurt, Germany
¹⁵Institute of Physics, Bhubaneswar 751005, India
¹⁶Indian Institute of Technology, Mumbai, India
¹⁷Indiana University, Bloomington, Indiana 47408
¹⁸Institut de Recherches Subatomiques, Strasbourg, France
¹⁹University of Jammu, Jammu 180001, India
²⁰Kent State University, Kent, Ohio 44242
²¹Lawrence Berkeley National Laboratory, Berkeley, California 94720
²²Massachusetts Institute of Technology, Cambridge, MA 02139-4307
²³Max-Planck-Institut für Physik, Munich, Germany
²⁴Michigan State University, East Lansing, Michigan 48824
²⁵Moscow Engineering Physics Institute, Moscow Russia
²⁶City College of New York, New York City, New York 10031
²⁷NIKHEF, Amsterdam, The Netherlands
²⁸Ohio State University, Columbus, Ohio 43210
²⁹Panjab University, Chandigarh 160014, India
³⁰Pennsylvania State University, University Park, Pennsylvania 16802
³¹Institute of High Energy Physics, Protvino, Russia
³²Purdue University, West Lafayette, Indiana 47907
³³University of Rajasthan, Jaipur 302004, India
³⁴Rice University, Houston, Texas 77251
³⁵Universidade de Sao Paulo, Sao Paulo, Brazil
³⁶University of Science & Technology of China, Anhui 230027, China
³⁷Shanghai Institute of Applied Physics, Shanghai 201800, P.R. China
³⁸SUBATECH, Nantes, France
³⁹Texas A&M University, College Station, Texas 77843
⁴⁰University of Texas, Austin, Texas 78712
⁴¹Tsinghua University, Beijing, P.R. China
⁴²Valparaiso University, Valparaiso, Indiana 46383
⁴³Variable Energy Cyclotron Centre, Kolkata 700064, India
⁴⁴Warsaw University of Technology, Warsaw, Poland
⁴⁵University of Washington, Seattle, Washington 98195
⁴⁶Wayne State University, Detroit, Michigan 48201
⁴⁷Institute of Particle Physics, CCNU (HZNU), Wuhan, 430079 China
⁴⁸Yale University, New Haven, Connecticut 06520
⁴⁹University of Zagreb, Zagreb, HR-10002, Croatia

(Dated: February 9, 2020)

We present first measurements of charge-dependent two-particle autocorrelations on axial momentum-space difference variables $\eta_1 - \eta_2$ (pseudorapidity) and $\phi_1 - \phi_2$ (azimuth) for primary charged hadrons with $0.15 \leq p_t \leq 2$ GeV/c and $|\eta| \leq 1.3$ from Au-Au collisions at $\sqrt{s_{NN}} = 130$ GeV. We observe large-momentum-scale correlation structures not predicted by theory but consistent with evolution of hadron emission geometry with increasing centrality from one-dimensional fragmentation of color strings to bulk hadronization of a hadron-opaque medium.

PACS numbers: 24.60.-k, 24.60.Ky, 25.75.Gz

Correlation and fluctuation analyses of heavy ion collisions should play a prominent role in studies of the color medium produced in ultrarelativistic heavy ion collisions

at RHIC [1, 2, 3]. Specifically, *in-medium modification* of color-string fragmentation and hard parton scattering in heavy ion collisions affects large-momentum-scale (two-

particle momentum difference comparable to STAR detector acceptance) correlations. Large-scale correlations may result from initial-state multiple scattering [4, 5], in-medium dissipation [6] and fragmentation of the color medium to final-state hadrons (string fragmentation in p-p, fragmentation of the bulk medium in A-A). String fragmentation models [7] account for axial (η, ϕ) correlations in high-energy p-p collisions in terms of local conservation of transverse momentum and net charge (canonical suppression of net-momentum and net-charge fluctuations). The correspondence in A-A collisions is an open question. Predictions have been made of dramatic suppression of net-charge fluctuations in central A-A collisions as a signal of quark-gluon plasma formation [8].

In this Letter we report the first measurement in heavy ion collisions of the centrality dependence of two-particle *charge-dependent* (like – unlike charge-pair difference) number-density autocorrelations on *difference variables* $\phi_\Delta \equiv \phi_1 - \phi_2$ and $\eta_\Delta \equiv \eta_1 - \eta_2$. Results suggest that local charge conservation at hadronization plus increasing system density and spatial extent induce evolution with Au-Au centrality from one-dimensional (1D) *charge-ordering* on configuration space z (beam axis) $\rightarrow \eta$ to two-dimensional (2D) charge ordering on $(z, \phi_x) \rightarrow (\eta, \phi_p)$ (ϕ_x refers to configuration-space azimuth). Those results were not anticipated by theoretical models [5, 9]. This analysis is based on Au-Au collisions at $\sqrt{s_{NN}} = 130$ GeV obtained with the STAR detector at the Relativistic Heavy Ion Collider (RHIC).

Charge-dependent (CD) autocorrelations access the *isovector* structure of two-particle pair-number density $\rho(\vec{p}_1, \vec{p}_2)$, projected in this analysis onto axial momentum components $(\eta_1, \eta_2, \phi_1, \phi_2)$. Differential correlation analysis is achieved by comparing object and reference distributions, the former comprised of particle pairs taken from single events (sibling pairs), the latter of pairs taken from different but similar events (mixed pairs). The two-particle pair-number density correlation function and pair-number ratio distribution for arbitrary charge-pair type are then defined respectively by

$$\begin{aligned} C(\vec{p}_1, \vec{p}_2) &= \rho_{mix}(\vec{p}_1, \vec{p}_2) [r(\vec{p}_1, \vec{p}_2) - 1], \\ r(\vec{p}_1, \vec{p}_2) &= \rho_{sib}(\vec{p}_1, \vec{p}_2) / \rho_{mix}(\vec{p}_1, \vec{p}_2). \end{aligned} \quad (1)$$

In this analysis pair-number densities $\rho(a, b; \vec{p}_1, \vec{p}_2)$ for charge-pair combinations ($a = \pm, b = \pm$) were projected onto variable pairs (η_1, η_2) , (ϕ_1, ϕ_2) and difference variables $(\eta_\Delta, \phi_\Delta)$ as histograms of pair-number counts $n_{ab,ij} \simeq \epsilon_x \epsilon_y \rho(a, b; x_i, y_j)$, where ϵ_x, ϵ_y are bin widths on variables $x, y \in \{\eta, \phi, \eta_\Delta, \phi_\Delta\}$. Sibling and mixed pair-number counts for each charge-pair type were separately normalized to the total number of detected pairs in each event class: $\hat{n}_{ab,ij} = n_{ab,ij} / \sum_{ij} n_{ab,ij}$. Normalized pair-number ratios $\hat{r}_{ab,ij} = \hat{n}_{ab,ij,sib} / \hat{n}_{ab,ij,mix}$ are the basis for this analysis. To reduce systematic error, pair-number ratio histograms were obtained for subsets of events with similar centrality (multiplicities in acceptance differ by ≤ 50) and primary-vertex location (within 7.5 cm along beam axis). Normalized ratios $\hat{r}_{ab,ij}$ for each

charge-pair type and centrality were formed as weighted averages over all subsets in the centrality class. Pair-number ratio histograms were obtained for like-sign (LS: $a = b$), unlike-sign (US: $a \neq b$), and charge-dependent (CD: LS – US) charge combinations [10].

Data for this analysis were obtained with the STAR detector [11] using a 0.25 T uniform magnetic field parallel to the beam axis. A minimum-bias event sample required coincidence of two zero-degree calorimeters (ZDC); a 15%-central event sample was defined by a threshold on the central trigger barrel (CTB), with ZDC coincidence. Event triggering and charged-particle measurements with the time projection chamber (TPC) are described in [11]. Tracking efficiencies, event and track quality cuts and primary-particle definition are described in [10, 12]. Particles were not identified. Corrections were made to $\hat{r}_{ab,ij}$ for two-track inefficiencies due to overlapping space points in the TPC (merging) and intersecting trajectories reconstructed as > 2 particles (splitting). Small-scale correlations due to quantum statistics, Coulomb and strong-interaction effects [13] were suppressed by eliminating sibling and mixed track pairs ($\hat{22}\%$ of total) with $|\eta_\Delta| < 1.0$, $|\phi_\Delta| < 1.0$, $|p_{t1} - p_{t2}| < 0.2$ GeV/c (transverse momentum), when either particle had $p_t < 0.8$ GeV/c. Four centrality classes (labeled (a) - (d) from central to peripheral) were defined by cuts on TPC track multiplicity N within the acceptance for this analysis ($|\eta| \leq 1.3$ and $0.15 \leq p_t \leq 2$ GeV/c) relative to endpoint N_0 [10, 14]. The more peripheral two centrality classes (d) and (c), totaling 122k events from the minimum-bias sample, were defined by $0.029 < N/N_0 \leq 0.21$ and $0.21 < N/N_0 \leq 0.56$ respectively. The more central two classes (b) and (a), totaling 178k events from the 15% most-central event sample, were defined by $0.56 < N/N_0 \leq 0.79$ and $0.79 < N/N_0$ respectively.

Fig. 1 shows pair-number ratios $\hat{r}_{ab,ij}$ on (η_1, η_2) and (ϕ_1, ϕ_2) for LS (left) and US (right) charge combinations in centrality class (a). Deviations from unity are typically a few *permil* for central Au-Au collisions. Quadrupole or v_2 number-density anisotropy (conventionally associated with elliptic flow) plus additional same-side ($|\phi_\Delta| < \pi/2$) enhancements dominate structure on ϕ_Δ in the lower panels. The anticorrelated LS and correlated US distributions on pseudorapidity difference variable η_Δ in the upper panels resemble pseudorapidity correlations in p-p collisions and are suggestive of charge-ordering in color string fragmentation [7, 16]. However, that interpretation is inaccurate for central A-A collisions – a more complete picture is obtained from 2D *joint* autocorrelations on combined variables $(\eta_\Delta, \phi_\Delta)$.

Invariance of correlation structure on sum variables $\eta_1 + \eta_2$ and $\phi_1 + \phi_2$ seen in Fig. 1 implies that those distributions can be projected onto respective difference variables to form 1D *autocorrelation histograms* without loss of information. 2D joint autocorrelations on difference-variable pair $(\eta_\Delta, \phi_\Delta)$ then compactly represent all correlation information on momentum subspace

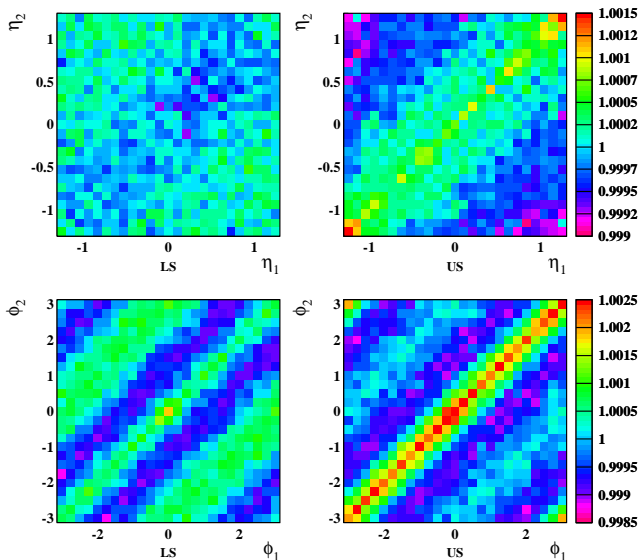


FIG. 1: Normalized pair-number ratios $\hat{r}_{ab,ij}$ for collisions in centrality class (a) (most central) for (η_1, η_2) (upper panels) and (ϕ_1, ϕ_2) (lower panels), and for like-sign (left panels) and unlike-sign (right panels) charge pairs within the full acceptance for this analysis. Color legends quantify amplitudes.

$(\eta_1, \eta_2, \phi_1, \phi_2)$. Perspective views of charge-dependent joint autocorrelations for variable $\bar{N}(\hat{r}_{ij} - 1)$ [\bar{N} is the ensemble mean multiplicity in acceptance] and four centrality classes are shown in Fig. 2. The vertical scale was chosen to emphasize the large-scale structure. Significant centrality dependence is observed along both pseudorapidity and azimuthal difference variables. Distributions are dominated by a 2D negative peak: broader and elliptical for peripheral collisions, with major axis along ϕ_Δ , transitioning smoothly to a narrower and deeper peak nearly symmetric on $(\eta_\Delta, \phi_\Delta)$ for central collisions. 1D projections onto difference variables ϕ_Δ and η_Δ are shown in Fig. 3. Solid dots (open triangles) correspond to η_Δ (ϕ_Δ) projections. The projections show that with increasing centrality the 2D peak exhibits 1) strong amplitude increase, 2) significant width reduction and 3) transition to approximately equal widths on ϕ_Δ and η_Δ .

Statistical errors for 2D joint autocorrelations are uniform on ϕ_Δ (because periodic) but approximately double as $|\eta_\Delta|$ increases from 0 to 2. Statistical errors for $\hat{r}_{ab,ij}$ at $|\eta_\Delta| = 0$ vary from 0.0002 for central collisions to 0.002 for peripheral collisions, whereas statistical errors for $\bar{N}(\hat{r}_{ab,ij} - 1)$ (~ 0.2) are approximately independent of centrality. Systematic errors were estimated as in [10]. Systematic uncertainty in the two-track inefficiency correction was estimated by Monte Carlo simulation [17] using measured two-track inefficiencies and determined to be negligible except in the region defined by $|\phi_\Delta| \leq 0.8$ and $|\eta_\Delta| \leq 0.04$. Correlations from resonance (ρ^0, ω) decays were estimated to be about 10% of the peaks in Fig. 2 in the range $|\eta_\Delta| < 0.5$, $|\phi_\Delta| < 2$ [17].

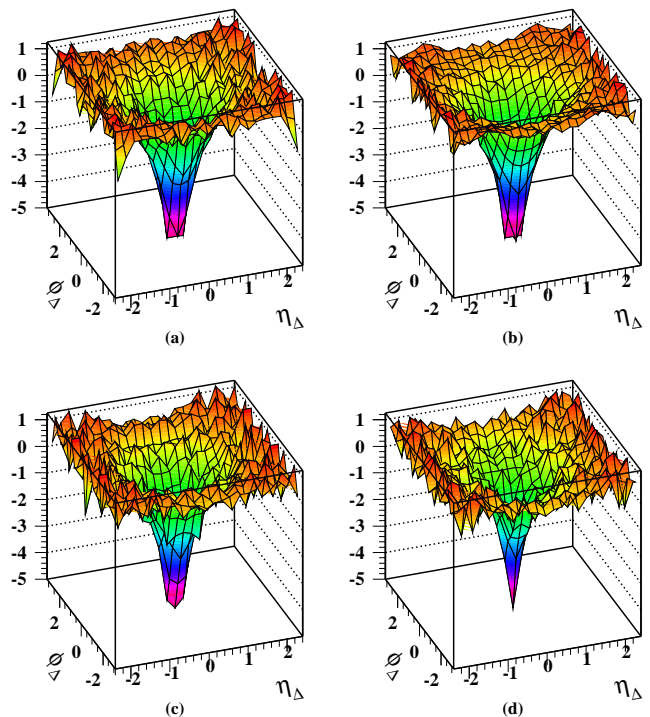


FIG. 2: Perspective views of two-particle CD joint autocorrelations $\bar{N}(\hat{r}_{ij} - 1)$ on $(\eta_\Delta, \phi_\Delta)$ for central (a) to peripheral (d) collisions. Center bins at $\phi_\Delta = \eta_\Delta = 0$ were omitted from model fits, as discussed in the text.

Joint autocorrelations in Fig. 2 were fitted with a two-component model function (plus constant offset) to quantify the centrality dependencies noted in Figs. 2 and 3. The model function consists of a 2D function peaked on both η_Δ and ϕ_Δ and a 1D gaussian peaked only on η_Δ (motivated by the p-p limiting case [16, 18]) written as

$$F = A_0 + \sum_{k=1}^2 A_k e^{-\left[\left(\frac{\phi_\Delta}{\sqrt{2}\sigma_{\phi_\Delta,k}} \right)^2 + \left(\frac{\eta_\Delta}{\sqrt{2}\sigma_{\eta_\Delta,k}} \right)^2 \right]^{P_k/2}}, \quad (2)$$

where $k = 1$ corresponds to the dominant 2D peak on $(\eta_\Delta, \phi_\Delta)$, with $P_1 = 1$ reflecting the exponential shape of the observed peak. $k = 2$ corresponds to the independent gaussian peak on η_Δ ($\sigma_{\phi_\Delta,2} \rightarrow \infty$), with P_2 and $\sigma_{\eta_\Delta,2}$ fixed to 2 and 1.5 respectively. Best-fit values for the remaining parameters and χ^2/DoF for the four centralities are listed in Table I. Extrapolation factors \mathcal{S} for $\bar{N}(\hat{r}_{ab,ij} - 1)$ [10] provide corrections for background contamination and tracking inefficiency [12]. Systematic error in \mathcal{S} was estimated to be $\pm 8\%$. Total systematic error for extrapolated quantities in Table I was 11% (errors added in quadrature).

CD correlations for central Au-Au collisions differ markedly from p-p observations. In Au-Au collisions a large-amplitude 2D negative exponential peak dominates the correlation structure, with similar widths on η_Δ and ϕ_Δ much reduced from p-p collisions. CD correlations in the p-p collision system are dominated by a 1D gaussian

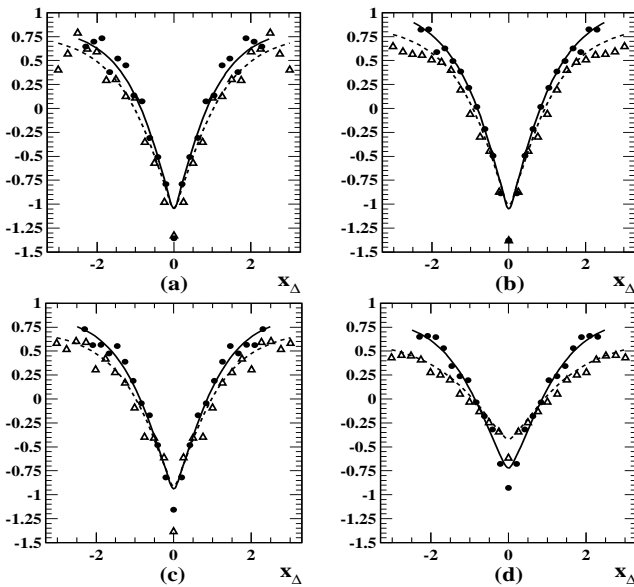


FIG. 3: Projections of 2D CD joint autocorrelations $\bar{N}(\hat{r}_{ij} - 1)$ in Fig. 2 onto difference variables η_Δ (solid points) and ϕ_Δ (open points) for central (a) to peripheral (d) collisions. Solid (dashed) curves represent corresponding projections of 2D analytical model fits to the data. 2D peaks are substantially reduced in amplitude by 1D projections.

TABLE I: Parameters and fitting errors (only) for model fits [Eq. (2)] to joint autocorrelation data in Fig. 2 for centrality bins (a) - (d) (central - peripheral). Total systematic error for normalized amplitudes is 11%.

centrality	(d)	(c)	(b)	(a)	error ^a (%)
S	1.19	1.22	1.25	1.27	8 ^b
\bar{N}	115.5	424.9	789.3	983.0	
SNA_0	0.98	0.80	0.91	0.79	11- 12
SNA_1	-4.1	-6.8	-7.7	-7.7	6-4
$\sigma_{\phi_\Delta,1}$	0.66	0.54	0.51	0.51	11-5
$\sigma_{\eta_\Delta,1}$	0.46	0.42	0.41	0.41	10-5
SNA_2	-0.51	-0.11	-0.15	-0.021	0.17-0.19 ^c
χ^2/DoF	$\frac{380}{315}$	$\frac{315}{315}$	$\frac{314}{315}$	$\frac{329}{315}$	

^aRange of fitting errors in percent from peripheral to central.

^bSystematic error.

^cMagnitude of fitting errors.

peak on η_Δ with $\sigma_{\eta_\Delta} \simeq 1$ [16, 18], associated with charge ordering on z during string fragmentation [7] expressed on pseudorapidity η through Bjorken expansion. For the most peripheral Au-Au events, in centrality class (d), we observe a change in CD correlation structure suggesting asymptotic approach to p-p collisions. Variation of peak amplitudes and widths with Au-Au centrality are shown in Fig. 4, along with p-p limiting cases (bands and line). STAR p-p data at 200 GeV [18] included in Fig. 4 ($\nu = 1$) are consistent with ISR p-p data at 52.5 GeV [16].

We speculate that the phenomenon driving CD correlations in Au-Au collisions remains local-in-configuration-space charge ordering, but that the hadronization geometry changes from 1D in p-p to 2 or higher dimensions

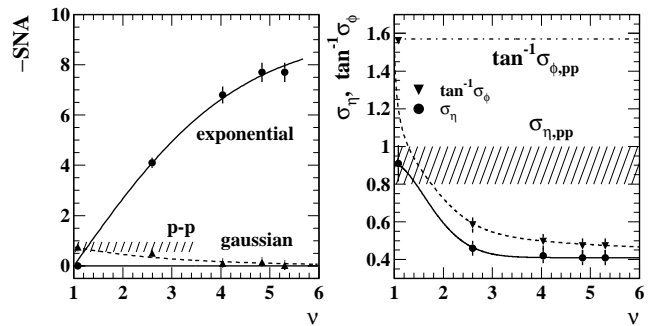


FIG. 4: Left panel: Amplitudes for exponential (dots) and Gaussian (triangles) peak components from Table I for peaks in Fig. 2 are plotted on mean path length ν [14]. Right panel: Fitted widths σ_{η_Δ} (dots) and $\tan^{-1} \sigma_{\phi_\Delta}$ (triangles) are also plotted on ν . Hatched regions, dash-dot line and $\nu = 1$ data points summarize p-p limiting values. Curves guide the eye.

with increasing A-A centrality, and that a hadron-opaque medium forms in the more central Au-Au collisions. In Figs. 2 - 4 1D charge ordering appears to be sharply reduced already for rather peripheral Au-Au collisions ($\nu \sim 2$). The exponential peak shape on pair opening angle, with small and equal correlation lengths on η_Δ and ϕ_Δ for central collisions, suggests that observation of CD correlations depends on a hadron mean free path, that CD correlations are detected only if both particles in a correlated pair are not absorbed or significantly scattered in the medium. This interpretation implies that the CD correlation is a bulk phenomenon and not due to parton fragmentation outside the medium. The possibility that the exponential peak structure arises from charge ordering in jet fragmentation was tested by splitting the Au-Au data at $p_t = 0.5$ GeV/c, below which jet fragments are expected to be negligible. The peak structures in Fig. 2 are observed to dominate both subsamples, although there are quantitative differences.

HIJING [5] and RQMD [9] exhibit isovector (CD) axial correlations (respectively consistent with 1D string fragmentation and resonance decays) which qualitatively fail to describe the present results. Hijing isovector correlations are determined by the Lund model in Pythia, and are therefore consistent with p-p results for all A-A centralities: Gaussian peak on η_Δ and no structure on ϕ_Δ . The amplitude is about 10% of the peak in Fig. 2 (a). RQMD, dominated by resonance decays and hadronic rescattering, exhibits a broad 2D Gaussian on $(\eta_\Delta, \phi_\Delta)$ with amplitude again about 10% of data for central events. Large-scale correlations in the data of Fig. 1 for both US and LS pairs are consistent with local charge ordering but inconsistent with CD correlations from decay of hadronic resonances such as the ρ^0 , which would affect only the US pair type, further arguing against a resonance gas scenario for these correlations.

Predictions of large ($\sim 4x$) suppression of net-charge fluctuations in connection with QGP formation [8] can also be tested with these data. Net-charge fluctuations

are measured by *integrals* of corresponding CD autocorrelations [19]. Integrating each of the observed Au-Au CD peak structures using the peak parameters in Table I we find that the integrals increase linearly in magnitude on ν by only 20%, are consistent with p-p results when extrapolated to $\nu = 1$ and are qualitatively inconsistent (magnitude too small) with predictions of dramatic fluctuation suppression. Large net-charge fluctuation suppression would imply very strong spatial correlation of charge pairs which should manifest in a highly-structured CD autocorrelation, especially a dramatic variation of the autocorrelation integral with centrality. The present peak-integral results exclude variation of the expected canonical suppression by more than a few tens of percent; however, the peak *shape* does change dramatically, reflecting the change in hadronization geometry.

We have measured charge-dependent joint autocorrelations on difference variables ϕ_Δ and η_Δ for Au+Au collisions at $\sqrt{s_{NN}} = 130$ GeV. The data are consistent with local charge conservation or canonical suppression of net charge fluctuations, evolving from 1D color-string frag-

mentation in p-p collisions to exponentially-attenuated ≥ 2 D charge-ordered emission from a hadron-opaque medium in central Au-Au collisions. These results are qualitatively inconsistent with standard collision models and predictions of QGP-related strong suppression of net-charge fluctuations. Charge-dependent autocorrelations provide unique access to the geometry of hadronization and rescattering as the energy density and spatial extent of A-A collisions increase with centrality.

We thank the RHIC Operations Group and RCF at BNL, and the NERSC Center at LBNL for their support. This work was supported in part by the HENP Divisions of the Office of Science of the U.S. DOE; the U.S. NSF; the BMBF of Germany; IN2P3, RA, RPL, and EMN of France; EPSRC of the United Kingdom; FAPESP of Brazil; the Russian Ministry of Science and Technology; the Ministry of Education and the NNSFC of China; Grant Agency of the Czech Republic, FOM and UU of the Netherlands, DAE, DST, and CSIR of the Government of India; Swiss NSF; and the Polish State Committee for Scientific Research.

-
- [1] R. Stock, Nucl. Phys. **A661**, 282 (1999); H. Heiselberg, Phys. Rep. **351**, 161 (2001).
- [2] A. Dumitru, R. Pisarski, Phys. Lett. **B504**, 282 (2001).
- [3] L. M. Bettencourt, K. Rajagopal and J. V. Steele, Nucl. Phys. **A693**, 825 (2001).
- [4] M. Gaździcki, A. Leonidov, G. Roland, Eur. Phys. J. **C6**, 365 (1999).
- [5] X.N. Wang, M. Gyulassy, Phys. Rev. D **44**, 3501 (1991).
- [6] Q. Liu and T. A. Trainor, Phys. Lett. **B567**, 184 (2003).
- [7] B. Andersson, G. Gustafson, G. Ingelman and T. Sjöstrand, Phys. Rep. **97**, 31-145 (1983).
- [8] M. Asakawa, U. Heinz, B. Müller, Phys. Rev. Lett. **85**, 2072 (2000); S. Jeon, V. Koch, Phys. Rev. Lett. **85**, 2076 (2000).
- [9] H. Sorge, H. Stöcker, W. Greiner, Nucl. Phys. **A498**, 567c (1989); Ann. Phys. (N.Y.) **192**, 266 (1989).
- [10] J. Adams *et al.* (STAR Collaboration), eprint nucl-ex/0308033.
- [11] K. H. Ackermann *et al.*, Nucl. Instrum. Meth. A **499**, 624 (2003); see other STAR papers in volume **A499**.
- [12] C. Adler *et al.*, Phys. Rev. Lett. **87**, 112303 (2001); *ibid.* **89**, 202301 (2002).
- [13] C. Adler *et al.* Phys. Rev. Lett. **87**, 082301 (2001).
- [14] Quantity $\nu \simeq 5.5 (N_{part}/N_{part,max})^{1/3} \simeq 5.5 (N/N_0)^{1/3}$ estimates mean participant path length as a number of encountered nucleons. N_0 is the half-maximum end point of the minimum-bias distribution plotted as $d\sigma/dN_{ch}^{1/4}$.
- [15] Quantities $\bar{N}(\hat{r}_{ab,ij} - 1)$ measure *per particle* correlations and are typically $O(1)$ for all centralities.
- [16] D. Drijard *et al.* [ACCDHW Collaboration], Nucl. Phys. B **166**, 233 (1980).
- [17] R. Ray and R. Longacre, nucl-ex/0008009, unpublished.
- [18] R. J. Porter and T. A. Trainor (STAR Collaboration), eprint hep-ph/0406330
- [19] T. A. Trainor, hep-ph/0001148 (unpublished).